

# Stress-induced phase transformations in Ti-15Mo alloy at elevated temperature

Petr Harcuba<sup>a</sup>, Tomáš Krajňák<sup>a,b\*</sup>, Dalibor Preisler<sup>a</sup>, Jiří Kozlík<sup>a</sup>, Josef Stráský<sup>a</sup>, Jana Šmilauerová<sup>a</sup>, Fernando Gustavo Warchomicka<sup>c</sup>, Miloš Janeček<sup>a</sup>

<sup>a</sup> Charles University, Faculty of Mathematics and Physics, Ke Karlovu 3, 12116 Prague, Czech Republic

<sup>b</sup> Research Centre, University of Žilina, Univerzitná 1, 01026 Žilina, Slovakia

<sup>c</sup> Graz University of Technology, Inst Mat Sci Joining & Forming, A-8010 Graz, Austria

## Abstract

Controlled mechanical loading was applied to Ti-15Mo alloy during annealing at 550 °C. Massive formation of the  $\omega_{\text{iso}}$  phase from the parent  $\beta$ -phase occurred during annealing at 550 °C without external stress or with stress well below the yield stress. Moreover, a massive  $\alpha$  phase precipitation takes place under simultaneous annealing and plastic deformation. Plastic deformation plays a key role in  $\beta \rightarrow \alpha$  transformation and achieving refined  $\alpha + \beta$  type microstructure resulted in improved mechanical properties. Studying phase transformations during plastic deformation is critical for understanding and optimizing thermomechanical processing of metastable  $\beta$ -Ti alloys.

**Keywords:** Ti-15Mo alloy, phase transformations, thermo-mechanical testing

## 1. Introduction

Metastable  $\beta$ -Ti alloys exhibit high specific strength, excellent corrosion resistance, biocompatibility, low elastic modulus, good fatigue resistance and formability. The combination of the aforementioned properties predetermines this class of Ti-alloys for applications in the aerospace industry or biomedicine. Due to the metastable nature of the  $\beta$ -phase,  $\beta$ -Ti alloys undergo several phase transformations during annealing below the so-called  $\beta$ -transus temperature or upon cooling from the  $\beta$ -phase field to room temperature [1-3]. Growth of  $\omega$  phase [4] and precipitation of  $\alpha$  phase in the  $\beta$  matrix [5] are typical diffusion-enabled phase transformations taking place during exposure to elevated temperatures. Metastable  $\beta$ -Ti alloys also experience stress-induced and deformation-induced transformations, namely formation of stress-induced martensite. Deformation at elevated temperatures in the two-phase ( $\alpha + \beta$ ) region affects  $\alpha \leftrightarrow \beta$  transformation. Namely  $\alpha$ -phase precipitation, is important for practical applications, as hot working (extrusion, forging, etc.) is usually employed to tailor the microstructure, and  $\alpha + \beta$  two-phase microstructure usually exhibits best mechanical properties [6].

The deformation below the  $\beta$ -transus temperature and associated phase transformations with initial single  $\beta$  phase microstructure have been reported only rarely. Thermo-mechanical

---

\*Corresponding author

E-mail address: tomas.krajnak@matfyz.cuni.cz (T. Krajňák)

processing of Ti-6246 alloy cooled from the  $\beta$  field showed deformation induced  $\alpha$  formation, affected by defects acting as nucleation points [7,8]. Deformation induced  $\alpha$  phase was also observed with beta annealed microstructure heated up to 600-700 °C in Ti-7333 [9,10] and Ti-5553 [11,12] with very short soaking time. The authors observed a dynamic precipitation of alpha, following selected  $\alpha$  variant to nucleate in the beta field.

Among the  $\beta$ -Ti alloys, Ti-15Mo represents a simple binary system that has been extensively studied in the last decade. Most of the studies focused on diffusional phase transformations during/after annealing without external stress. Only Wang et al. investigated stress-induced  $\beta \rightarrow \omega$  phase transformations in cold-drawn Ti-15Mo wires [13].

This study investigates the influence of applied stress and deformation on phase transformations in the Ti-15Mo alloy at the elevated temperature of 550 °C. The temperature was selected as it is just below the  $\omega$ -solvus temperature, while a complete dissolution of  $\omega_{iso}$  particles occurs at the temperature of 560 °C [14,15]. In a stress/strain-free condition,  $\alpha$  phase does not precipitate upon the annealing treatment used in this study, allowing us to reveal the effect of stress and deformation on the  $\beta \rightarrow \alpha$  transformation.

## 2. Experimental procedure

Ti-15Mo alloy (Carpenter Technology Co., USA) contained 15 wt% of Mo and the content of oxygen and nitrogen was 0.185 wt% and 0.014 wt%, respectively. First, the material was encapsulated in a fused quartz (Ar atmosphere), solution treated at 900 °C for 4 h and immediately quenched in water. Samples of a cylindrical shape with the diameter of 10 mm and the height of 15 mm were subjected to three thermo-mechanical tests in the Gleeble® 3800 system. All samples were heated at 50 °C/min up to 550 °C, kept at this temperature for 10 min and water quenched to room temperature. The temperature was controlled by a K-thermocouple spot-welded directly to the sample. The first sample was heat-treated under minimal applied stress (0 MPa), the second one under elastic stress of 200 MPa. The third sample was heated to 550 °C and compressed to the true strain of 0.5 at the true strain rate of  $10^{-3} \text{ s}^{-1}$  (referred to as Deformed). The duration of the deformation and thus the time spent at the elevated temperature was also 10 min.

The microstructure of the samples was investigated by the Apreo 2 (Thermo Fisher Scientific) SEM operated at 2 keV to minimize the interaction volume and to allow the observation of clear and sharp fine particles. X-ray diffraction (XRD) was performed using the Rigaku Rapid II diffractometer in the reflection geometry using a curved 2D plate detector and a sealed Mo tube X-ray source with the spot size of 0.3 mm. XRD patterns were obtained by integrating the measured Debye-Scherrer rings. The microstructure investigation was complemented by Vickers microhardness measurement under a load of 500 g and a dwell time of 10 s. 25 indents were made and evaluated by an automatic microhardness tester Qness Q10a. The sample preparation consisted of mechanical grinding using SiC papers with decreasing grit size down to the #2000, followed by polishing using a 20% solution of hydrogen peroxide in the OP-S colloidal silica suspension.

## 3. Experimental results and discussion

The microstructure of the reference ST sample (not presented here) consists of large  $\beta$  grains and nano-sized coherent particles of  $\omega$  athermal ( $\omega_{ath}$ ) phase [4]. BSE SEM

micrographs of heat-treated samples are shown in Fig. 1. The microstructures of the sample annealed without external stress (0 MPa) (Fig. 1a) and the sample elastically loaded during annealing (200 MPa) (Fig. 1b) are similar. Only a low amount of thin  $\alpha$  lamellae with a very high aspect ratio can be observed, mainly along grain boundaries. Numerous fine particles (ellipsoids of the size in the range of tens of nm) uniformly dispersed in the  $\beta$ -matrix of both samples were identified by subsequent XRD measurements as the  $\omega_{iso}$  phase. Based on image analysis, the sample elastically loaded at 200 MPa exhibits higher number of  $\omega_{iso}$  particles, while having comparable volume fraction of around 10 %. However, minor differences in observed density, size and shape may not be significant as the appearance of  $\omega_{iso}$  particles differs in each grain due to its orientation w.r.t. to the sample surface. Few elongated  $\alpha$  phase particles can also be found in both samples, namely close to  $\beta/\beta$  grain boundaries. On the other hand, completely different microstructure with a high fraction of tiny  $\alpha$  phase particles were observed in the sample deformed in compression, appearing dark in the SEM image shown in Fig. 1f.

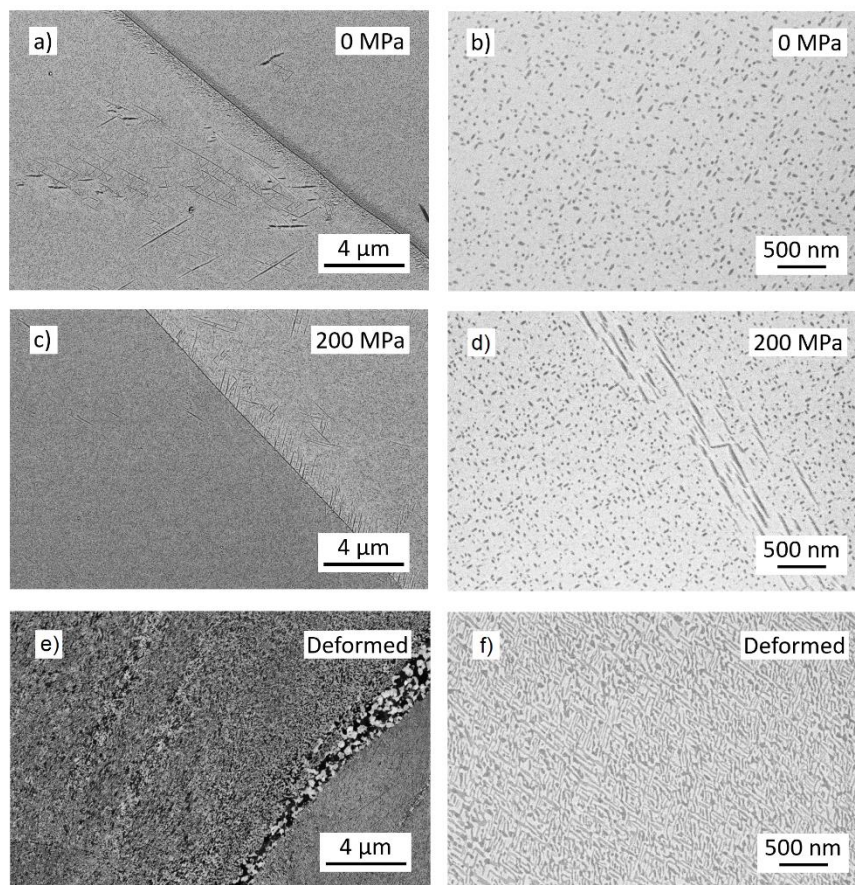


Fig. 1- A backscatter SEM micrographs of the samples annealed at 550 °C for 10 min (a,b) at 0 MPa, (c,d) under elastic load of 200 MPa and (e,f) deformed in compression (10 min). Loading direction is horizontal.

The phase composition of the samples was determined by XRD. XRD patterns of all investigated states are shown in Fig. 2. The pattern of the ST sample shows narrow  $\beta$  matrix peaks and small and very broad peaks due to nanometer-sized  $\omega_{ath}$  particles. After annealing without load (0 MPa), formation of the  $\omega_{iso}$  phase is demonstrated by more pronounced  $\omega$

phase peaks. The intensity of the  $\omega_{\text{iso}}$  peaks further, though only slightly, increased after annealing with the applied elastic load of 200 MPa (see the cyan arrow in Figure 2), indicating that the fraction of the  $\omega_{\text{iso}}$  phase increases compared to the 0 MPa sample. On the other hand, no  $\omega_{\text{iso}}$  phase was detected in the deformed sample. The microstructure of the deformed sample consists only of  $\alpha$  and  $\beta$  phases (magenta arrows in Figure 2).

Plastic deformation clearly promoted the  $\beta \rightarrow \alpha$  transformation in the deformed sample. The resulting microstructure is extremely fine with a large number of very small (less than 100 nm)  $\alpha$  particles. This is most likely caused by dislocation activity which facilitates nucleation and accelerates the growth kinetics of  $\alpha$  phase in the deformed condition/sample, as reported also in [9,12]. The morphology of  $\alpha$  particles resembles nearly the globularized microstructure, which can be obtained in Ti17 alloy from initial  $\alpha + \beta$  microstructure, using the same strain rate, but at much higher temperatures (e.g. 810 °C) [16]. Since the temperature of only 550 °C was used,  $\alpha$  particles with the size on the 10 nm scale precipitated in the Deformed sample.

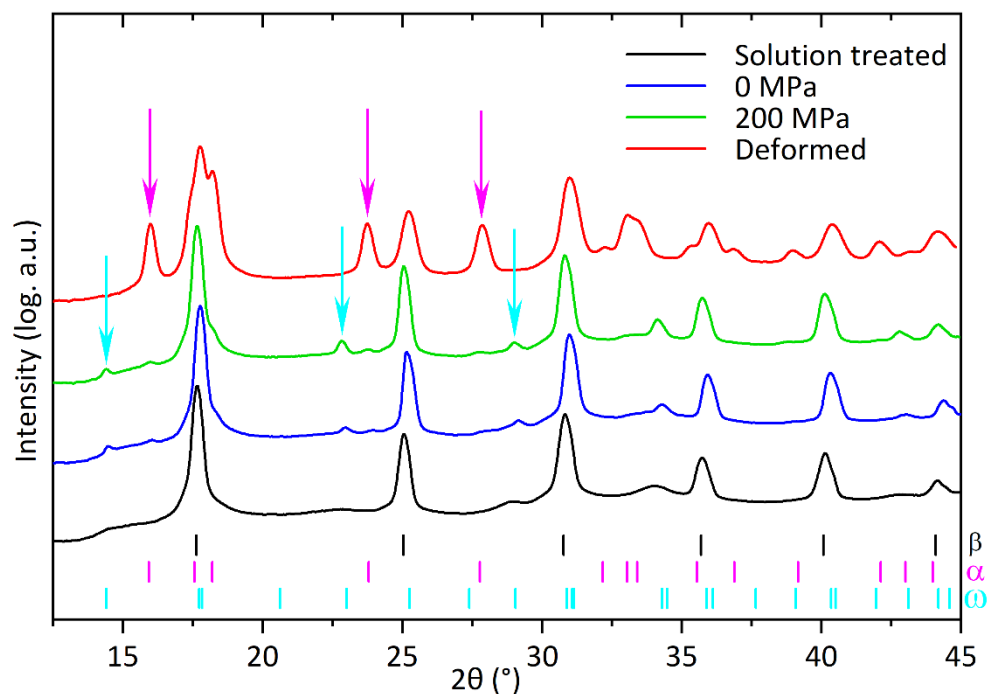


Fig. 2 Normalised XRD patterns of all conditions. The intensity is plotted in the logarithmic scale, and the patterns are shifted vertically for clarity. The positions of the peaks corresponding to  $\alpha$ ,  $\beta$  and  $\omega$  phases are indicated in the lower part of the graph. Magenta and cyan arrows point to the most distinct peaks of  $\alpha$  and  $\omega$  phases, respectively.

The effect of the phase composition on the mechanical properties of the metastable Ti-15Mo alloy was investigated by Vickers microhardness (HV) measurement. As it is apparent from the HV results plotted in Fig. 3, the microhardness of the ST sample increases from 309 HV to 344 HV upon annealing without stress (0 MPa). This can be attributed mainly to the  $\omega_{\text{iso}}$  phase formation, while the effect of the formation of sparse  $\alpha$  lamellae is minor. After annealing during elastic loading at 200 MPa, the microhardness increases to 368 HV due to the more pronounced  $\omega_{\text{iso}}$  phase precipitation. The deformed sample exhibits the highest microhardness of 398 HV, due to the refined  $\alpha + \beta$  microstructure [17]. Extremely fine

$\alpha$  particles result in high microhardness which is typical rather for  $\beta+\omega_{iso}$  phase composition [18].

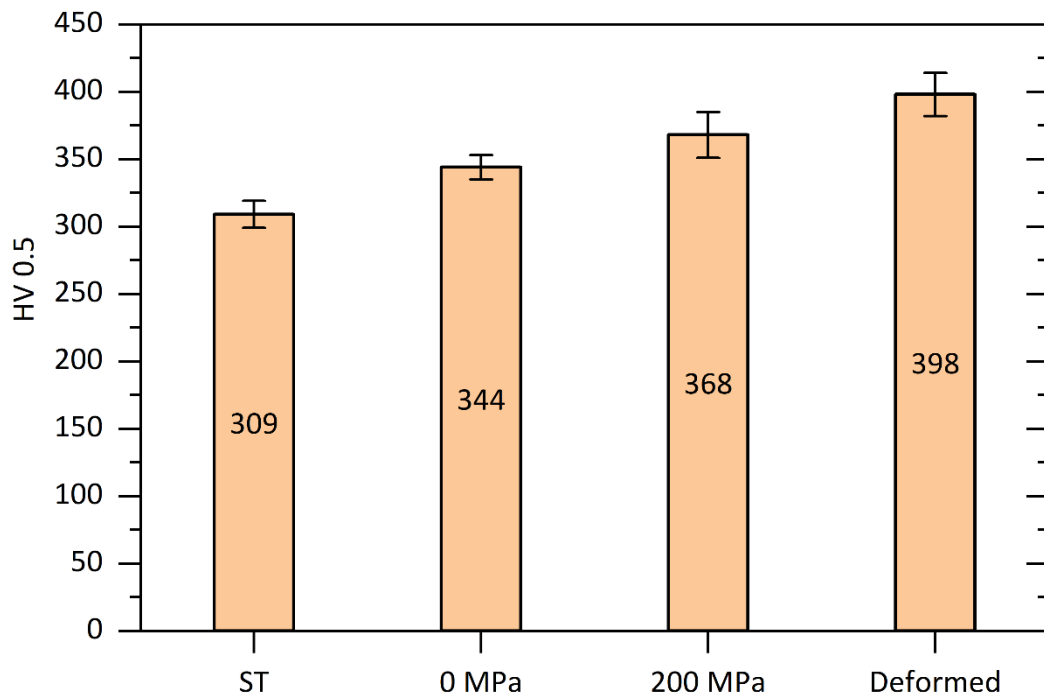


Fig. 3 Microhardness values measured for all investigated states.

## Conclusions

The influence of the mechanical loading on phase transformations in the solution treated Ti-15Mo alloy was investigated. The following conclusions can be drawn from this experimental study:

- Mechanical loading below yield stress of the material has a limited effect on phase transitions at 550 °C.
- Deformation applied during annealing promotes  $\alpha$  precipitation.
- Ultra-fine microstructure of  $\alpha$  particles smaller than 100 nm is formed.
- Microhardness increases from 309 HV (solution treated sample) to 398 HV (deformed sample).
- Careful temperature and deformation control may allow achieving unprecedented microstructural and mechanical conditions in metastable  $\beta$ -Ti alloys.

## Acknowledgements

Financial support by the Czech Science Foundation and the Austrian Science Fund under the joint project 22-21151K (CSF)/I 5818 (FWF) is gratefully acknowledged. P. H., T. K., D. P., J. K., J. S., J. Š. and M. J. gratefully acknowledge the partial financial support by OP Johannes Amos Comenius of the MEYS of the CR, project No. CZ.02.01.01/00/22\_008/0004591. The XRD measurements were performed in MGML (mgml.eu) within the program of Czech Research Infrastructures, project No. LM2018096.

## References

- [1] R. Kolli et al., *Metals* 8 (2018) 506. <https://doi.org/10.3390/met8070506>.
- [2] N. Yumak et al., *J. Mater. Res. Technol.* 9 (2020) 15360–15380. <https://doi.org/10.1016/j.jmrt.2020.10.088>.
- [3] J.W. Lu et al., *Mater. Charact.* 84 (2013) 105–111. <https://doi.org/10.1016/j.matchar.2013.07.014>.
- [4] P. Zháňal et al., *J. Mater. Sci.* 53 (2018) 837–845. <https://doi.org/10.1007/s10853-017-1519-2>.
- [5] H.M. Flower et al., *J. Mater. Sci.* 9 (1974) 57–64. <https://doi.org/10.1007/BF00554755>.
- [6] K. Bartha et al., *Mater. Today Commun.* 22 (2020) 100811. <https://doi.org/10.1016/j.mtcomm.2019.100811>.
- [7] A. Dehghan-Manshadi et al., *Mater. Sci. Eng. A* 552 (2012) 451–456. <https://doi.org/10.1016/j.msea.2012.05.069>.
- [8] T. Kitashima et al., *Metals* 11 (2021) 1405. <https://doi.org/10.3390/met11091405>.
- [9] K. Hua et al., *Int. J. Plast.* 119 (2019) 200–214. <https://doi.org/10.1016/j.ijplas.2019.03.011>.
- [10] K. Hua et al., *Mater. Des.* 197 (2021) 109275. <https://doi.org/10.1016/j.matdes.2020.109275>.
- [11] J. Fan et al., *Mater. Charact.* 130 (2017) 149–155. <https://doi.org/10.1016/j.matchar.2017.06.005>.
- [12] K. Hua et al., *Mater. Sci. Eng. A* 840 (2022) 142997. <https://doi.org/10.1016/j.msea.2022.142997>.
- [13] X. Wang et al., *MATEC Web Conf.* 321 (2020) 12015. <https://doi.org/10.1051/mateconf/202032112015>.
- [14] K. Bartha et al., *J. Alloys Comp.* 867 (2021) 159027. <https://doi.org/10.1016/j.jallcom.2021.159027>.
- [15] P. Zháňal et al., *Acta Phys. Pol. A* 128 (2015) 779–783. <https://doi.org/10.12693/APhysPolA.128.779>.
- [16] F. Ferraz et al., *Mater. Sci. Eng. A* 903 (2024) 146645. <https://doi.org/10.1016/j.msea.2024.146645>.
- [17] T. Krajňák et al., *Mater. Des.* 222 (2022) 111049. <https://doi.org/10.1016/j.matdes.2022.111049>.
- [18] T. Krajňák et al., *J. Mater. Res. Technol.* 23 (2023) 4527–4537. <https://doi.org/10.1016/j.jmrt.2023.01.215>.